The importance of rear pillar geometry on fastback wake structures.

Joshua Fuller.

Martin A Passmore (Corresponding Author)

Department of Aeronautical and Automotive Engineering, Stewart Miller Building, Loughborough University, Leicestershire, LE11 3TU, UK

Tel; +44 (0)1509 227264

Fax: +44 (0)1509 227 275

ttmap@lboro.ac.uk

The wake of a fastback type passenger vehicle is characterised by trailing vortices from the rear pillars of the vehicle. These vortices strongly influence all the aerodynamic coefficients.
Working at model scale, using two configurations of the Davis model with different rear pillar radii, (sharp edged and 10mm radius) the flow fields over the rear half of the models were investigated using balance measurements, flow visualisations, surface pressure and PIV (Particle Image Velocimetry) measurements.
For a small geometry change between the two models, the changes to the aerodynamic loads and wake flow structures were unexpectedly large with significant differences to the strength and location of the trailing vortices in both the time averaged and unsteady results. The square edged model produced a flow field similar to that found on an Ahmed model with a sub-critical backlight angle. The round edged model produced a flow structure dominated by trailing vortices that mix with the wake behind the base of the model and are weaker. This flow structure was more unsteady than that of the square edged model. Consequently, although both models can be described as having a wake dominated by trailing vortices, there are significant differences to both the steady state and unsteady flow fields that have not been described previously. This also shows that the fastback wake structure described by Ahmed is not definitive.

Wake, trailing vortices, unsteadiness, Davis model, Ahmed model, fastback

Notation

L – Model length
C_D - Drag Coefficient
C_D* - Drag Coefficient Standard deviation
C_L – Lift Coefficient
C_L* - Lift Coefficient standard deviation
C_{LR} – Rear Lift Coefficient
w – Distance from model centre line
W – Model width
h – Distance from floor
H – Model height
bl – Backlight length

1. Introduction

The structure of the wake at the rear of a road vehicle is widely known to be important in determining the overall aerodynamic characteristics of the vehicle; having a potential influence on the drag, the rear lift and hence stability and the unsteadiness of the overall flow-field. In the case of the fastback geometry the near wake is dominated by trailing vortices as identified by Morel (1978) and Ahmed *et al* (1984). These vortices can be responsible for a large proportion of total vehicle drag and strongly influence rear lift. When at yaw, acceleration of the air around the rear pillar into the trailing vortices, causes low pressure on the side of the vehicle which contributes to the overall side force and yaw moment, Howell and Baden Fuller (2010).

Since Ahmed's *et al* (1984) initial paper the flow structures around the Ahmed model have been investigated experimentally and using CFD in many studies, for example, Gilliéron and Chometon (1999), Guilmineau (2008), Krajnovic and Davidson (2005a) (2005b) and Lienhart and Becker (2003). The time averaged flow structures first identified by Ahmed have been more fully described in this work, but it is now also understood that the instantaneous flow fields around the model are quite different from the time averaged. A clear demonstration of this is given by Bearman (1997) showing some early PIV results and Sims-Williams (2001, 2003, 2006) who show that a wake dominated by trailing vortices can contain periodic features with the trailing vortex cores moving vertically and horizontally, alternately strengthening and shedding from the trailing edge of the backlight.

The Ahmed model has sharp edges on the intersections of the model surfaces at the rear but this does not accurately represent production vehicles, which often have significant curvature at the rear. Published research that uses models with rounded trailing edges is rare. Gilhaus and Renn (1986) showed that rounding the rear edges of a fastback car model reduced the drag coefficient and they commented on the sensitivity of the drag coefficient to this rear edge detail. Howell (1993) showed that rounding the rear edges of a simple car model altered the relationship between backlight angle and drag above the critical angle described by Ahmed. Buresti *et al* (1997) used an axisymmetric body and commented on the limited research into rear edge rounding. Because of this lack of published research, the applicability of the Ahmed body fastback flow structures to production vehicles is currently unknown, at least in the public realm.

Flow separation from curved surfaces is typically unsteady, controlling the separation is advantageous and this can be done using large scale design features to create sharp edges or with small, discrete strakes visually hidden in the rear pillars or rear light mouldings. These are found on a wide range of cars from small cars to large SUV's and there is a growing trend for their use. Dependent upon the physical location of the features they can be used to alter yaw moments, such as shown by Baden Fuller *et al* (2010), to reduce drag as demonstrated by Meyer and Wickern (2011) and Beaudoin and Aider (2008) or to change the lift as also demonstrated by Beaudoin and Aider (2008).

Passmore and Mansor (2006) show that a Davis model with a 20º backlight angle and a square cross section rear pillar has a steady-state yaw moment gradient 33% lower than the same model with 10mm radius on the rear pillars. Using the same models in a dynamic, oscillating yaw angle experiment, they also show that over a range of reduced frequencies, between 0.02 and 0.25, that the round edged model produced a steadier response than the square edged configuration. Both results are reasonably attributed to the rear pillar change; however the flow structures that caused these results were not investigated and while there is a body of research regarding wake structures more generally, there is no direct comparison of the effect of rear edge radius available in the literature.

The objective of this paper is to investigate the flow fields over the two 20º backlight angle Davis models used by Passmore and Mansor (2006) to demonstrate and describe the differences between the flow structures in a direct comparison. While it is clear, given the work of Ahmed *et al* (1984) and the wake surveys carried out by Davis (1982), that in both configurations the wake is likely to be dominated by trailing vortices, the extent of the changes associated with the small change in geometry is not clear. The analysis in this paper focuses on the relatively large scale

differences to the flows over the rear part of the models caused by the different rear pillar geometries, primarily the trailing vortices and the near wake, and concludes with sketches of the time averaged flow fields over the two models to clearly illustrate the changes and provide comparisons with published literature.

2. Models and Experimental Facilities

This research used two configurations of the 20º back-slant Davis model (Davis (1982)); in the first configuration all edges are rounded with a 10mm radius; the second is identical except for the rear pillars which have sharp, square edges. The basic model dimensions are shown in figure 1 and figure 2 shows an annotated schematic labelling the main model features. While the Davis geometry is not particularly representative of current road vehicles, the model was chosen for consistency with previous studies, in particular Passmore and Mansor (2006) where changes in the rear pillar radius were shown to be important in the yaw moment gradient. The model does, however, demonstrate the important flow-field features of a fastback road vehicle, for example, separation and reattachment on the slant, a twin counter rotating vortex structure and a turbulent wake downstream of the base (Davis (1982)).

[figure 1]

[figure 2]

Both model configurations were mounted on the centreline of the working section of the wind tunnel, 40 mm above the ground plane. A single Ø20mm shaft from the centre of the model's floor held the model in place and was connected through the wind tunnel floor to the under-floor balance.
Preliminary tests using both model configurations found the drag coefficient to be insensitive to Reynolds number (Re) above $Re = 1.3x10^6$ (30m/s) All the results in this paper were collected at 40m/s, giving $Re = 1.7x10^6$ based on model length.

All tests were conducted in Loughborough University's ¼ scale wind tunnel. This is an open circuit, closed working section wind tunnel. The working section has a fixed floor, $2.5m^2$ cross-section and a maximum wind speed of 45m/s with a freestream turbulence intensity of 0.2%; for more details see Johl *et al* (2004). The Davis model used in these tests gives a blockage ratio of 1.4%.

Although the fixed floor does not match the boundary layer conditions found under normal driving conditions Howell and Hickman (1997) show that the main effect of this is to change the absolute values of the aerodynamic loads, whilst the trends remain the same for both fixed and moving floors, this indicates that the large scale flow structures are largely independent of the floor boundary conditions.

Steady state aerodynamic loads were recorded with a six component under floor balance with accuracy in drag of 0.12N and lift of 0.5N. Balance data was collected for 30 seconds giving an accuracy of less than ± 0.001 C_D to 99% confidence. The six aerodynamic loads, defined by the Society of Automotive Engineers (SAE) sign convention, were converted to coefficients using the standard equations and a solid blockage correction (Carr 1982) was applied to all coefficients.

Surface flow visualisations used the traditional method of a mixture of titanium dioxide, paraffin and linseed oil. This was applied to the model surfaces and the tunnel was run at 40m/s until it had dried. The viscous nature of the visualisation mixture means that the instantaneous unsteadiness of the flow field is not recorded and the resultant patterns on the model represent the mean flow friction lines.

Surface pressures were recorded from an array of 122 pressure tappings arranged over each model, covering the backlight, both sides of the model below the rear pillar, and the model base, as shown in figure 3. On the slant and base there are seven rows located on the centre-line and at w/W= ±0.18, ±0.31 and ±0.40 with a longitudinal spacing of 20mm for the bottom half of the base and 30mm for the top. Along the pillars there are three rows of nine tappings on a 20mm by 20mm grid with the uppermost row aligned with the finish of the radius.

[figure 3]

The pressures were recorded using two 64 channel miniature pressure scanners and at each pressure tapping 8192 pressure samples were collected at 260Hz, representing 31 seconds of data. The pressure scanners had a manufacturer quoted accuracy of 1.47Pa. Pressure signal distortion caused by the tubing linking the model surface to the pressure scanner was removed using an experimentally derived correction function using a similar method as Sims-Williams and Dominy (1998). This was found by comparing a swept sine signal recorded through the length of tubing used in the model with the associated tail, to one recorded using a very short tube (≈15mm) to create a transfer function that describes the distortion created by the tubing. This removed the effects of a resonance in the tubing at 95Hz, reducing the magnitude of the pressure fluctuations around the mean value and allowed frequencies up to 130Hz to be accurately analysed. The surface pressures are presented as pressure coefficients based on freestream dynamic pressure and have been corrected for solid blockage (Carr (1982)).

Three component planar PIV data was collected in the y-z plane, 0.25L (156mm) behind the base of the model using a commercially available stereoscopic system, the setup is illustrated in figure 4. The 200mJ Nd:YAG pulsed laser was located above the working section and the two four-megapixel cameras were mounted at 60º to the laser sheet on supports within the working section. The angles of the camera lenses were adjusted using scheimpflug mounts. Seeding was provided by atomized olive oil distributed from a seeding rake upstream of the model; this increased the freestream turbulence to 4% which was the same for both models. The rake was only in place for the PIV data collection, all other data was collected in a clean wind tunnel.

[figure 4]

An inter-frame time of 30μs gave the best compromise between in-plane particle motion and the seeding particles passing through the laser sheet, producing an average pixel shift of the seeding particles of 5 pixels. Seeding was optimised to ensure that the processed data produced at least 85% first choice vectors, which is good considering the large field of view, and that the entire image was seeded. Image pairs were captured at 5Hz and each data set contained 1000 image pairs; this number has been shown by Passmore *et al* (2010) to give an accuracy of ±2% of the mean value with a 99% confidence of a vector towards the edge of a vortex. The images were processed using stereoscopic correlation in decreasing size multi-pass interrogation windows, starting with single passes at 128x128 and 64x64 pixels, then two passes at 32x32 with 50% overlap.

3. Results

Although the surface pressure and PIV data was collected across the entire width of the models, the results are presented as halves of a single figure to allow for a direct comparison of the rounded and sharp edged models. The left hand side of the figures contains results from the round edged model and those from the square edged model are on the right hand side. To ensure a true comparison and avoid any flow field asymmetry that might arise from the model manufacture, the results for the square edged model are also from the left hand side of the model but have been mirrored. This presentation is used throughout this paper and the sides of the plots are labelled throughout.

3.1 Steady State Results

The drag and lift coefficients of the two model configurations are in table 1; rear lift is given both as a coefficient and as a percentage of the total lift. These coefficients are calculated based on the SAE sign convention and using the standard equations.

[table 1]

The round edged model has lower drag and lift coefficients than the square edged model. On both model configurations, the majority of the lift originates from the rear of the model but despite higher overall lift on the square edged model, the balance of front and rear lift remained near constant. Sharpening the rear pillars increases the drag on this model, rather than reducing it as shown by Meyer and Wickern (2011) and this is due to the location of the geometry changes. Strakes used to reduce drag are generally on the vertical rear edges of a vehicle, rather than the edges of the backlight, and act to limit flow acceleration around the rear edge of the vehicle which would otherwise create a local area of low pressure and hence drag on the vehicle base.

The surface flow visualisations produced useful results but some of the features are relatively weak and the photographs do not reproduce well. Therefore sketches of the friction lines and critical points have been produced instead to give a much clearer representation; figure 5 shows the round edged model and figure 6 shows the square edged model.

Figure 5 shows two areas of recirculation (r1) below the backlight header, one on each side of the centreline. These are fed by flow from the corners of the roof and spiral towards separation points in the centre. These are bounded by flow lines created by saddle points on the roof trailing edge and 1/3 of the way down the centreline of the backlight (s1). These structures are likely to be very similar to those described by Spohn and Gillieron (2002).
For the first 1/4 of the rear pillars the flow remains attached, flowing from the side of the model around the rear pillars onto the backlight. Below this the flow separates; the separation line (s2) curves around the rounded rear pillar and further down the rear pillar splits; between these separation lines would be a secondary vortex, similar to that found on a delta wing (Houghton and Carpenter 2003), but there is no direct evidence of this visible on the model.
The reattaching flow (r2) from the trailing vortices extend towards the model centre line and only a small amount of flow travelled down the backlight to separate from the trailing edge on the model centreline.

[figure 5]

On either side of the model centreline on the base of the model is a weak, semi-circular structure (b1). The directions of these flow structures are unclear from the visualisation photographs; they just show that the paint has migrated away from the indicated line. These are only found on the base of the round edged model; there are no clear features on the base of the square edged model where the brush strokes still remained after 5 minutes of the wind tunnel running. It is unclear what is causing this flow pattern, Ahmed et al proposed a torus flow around the edges of the base, but no flow patterns are seen on the square edged model base which has geometry closer to that of the Ahmed model. This implies that the flow structures around the rear of the round edged model are different from those over the Ahmed model and the circular shape of the structures implies a link with the trailing vortices.

The sketch of the friction lines seen from a flow visualisation of the square edged model is in figure 6.

[figure 6]

As with the round edged model there are two recirculations (r1) at the top of the backlight which spiral towards the centre bounded by a saddle point (s1) on the backlight. The trailing vortices are present from the top of the trailing pillars separating from the sharp edge of the trailing pillar (s2); there is a second separation line slightly inboard of the edge. Between these there is evidence of a weak secondary vortex (v1). Unlike on the round edged configuration, both the separation line and the secondary vortex are located only on the backlight and do not wrap around the rear pillar. Both of these effects are a result of the square rear pillars creating a fixed flow separation point, independant of surface velocity ensuring that the flow on the side of the model remains attached and limiting the seperated flow to the backlight.
Compared to the round edged model, the trailing vortices do not extend as far inboard (r2) and more flow travels down the centreline of the model.
For the square edged model there are no discernible flow patterns on the base of the model.

Mean surface pressure coefficients on the rear half of the two model configurations are in figure 7. The different faces are arranged in a net centred on the backlight.

[figure 7]

The contributions to the overall drag and lift from the pressure tapped surfaces were found by integrating the surface pressure over the surrounding area; these have been converted to force coefficients and presented in table 2. Considering the spacing between the pressure tappings and the high pressure gradients under the trailing vortices, these values should be taken as representative rather than absolute of the contributions from each surface.

[table 2]

As with the balance measurements, higher lift and drag coefficients are found on the square edged model. The main differences in the forces between the two models occur on the backlight whereas the difference in base drag is very small.

The general trends of the pressure distributions are the same for the two model configurations but the details are quite different.
At the backlight header of both model configurations is an area of low pressure caused by flow accelerating from the roof onto the backlight but there is no distinct evidence of the recirculation seen in the surface flow visualisation, indicating that these structures are very weak and do not extend far from the model surface.
Along the backlight centreline of both model configurations is pressure recovery as the body tapers. Towards the trailing edge of the backlight the pressure recovery stops, influenced by the trailing vortices leaving the trailing edge of the backlight and the base wake.
Lower pressures are found at the edges of the backlight and higher pressures on the centreline. The low pressures along the edges are caused by high flow velocity under the trailing vortices but, unlike in the flow visualisation, the exact locations of the vortices on the backlight are unclear due to the pressure tapping resolution. The pressures on the edge of the backlight of the square edged model configuration are lower than on round edged model configuration indicating more intense vortices, in agreement with the flow patterns in figure 5.
Across most of the backlight, the pressures on the square edged model are lower than those on the round edged model, caused by higher central downwash speeds over most of the backlight; this is a direct consequence of the stronger trailing vortices drawing more flow onto the backlight.
At the trailing edge of the backlight of the round edged model configuration is a small region of low pressure caused by the trailing vortex leaving the backlight. This correlates with the lateral location of the weak flow features found on the base of the model, in figure 5.

In the lower corner of the backlight of the square edged model configuration is a triangle of low pressure extending from the low pressure along the backlight edges under the trailing vortices. This is caused by the trailing vortices expanding as they leave the backlight.
The base pressures on both models are around -0.1Cp, with little variation across the width, this indicates fully separated flow. The weak feature seen on the base of the round edged model, figure 5, is not seen probably due to the pressure tapping resolution on the base.

On the sides of both model configurations the pressures decrease towards the backlight edge with the sides of the round edged model showing a steeper pressure gradient, indicating greater flow acceleration, than the square edged model. The largest pressure gradient and flow accelerations on the square edged model occur on the backlight, showing that the flow acceleration into the trailing vortices happens on the backlight rather than on the sides of the model. This agrees with the different locations of the separation lines seen in the flow visualisation on the two models in figures 5 and 6.

Vectors of the mean in-plane velocities behind the two models in a plane 0.25L behind the model are in figure 8.
All the PIV results include a simplified model outline and the dimensions are non-dimensionalised with model width on the x-axis and model height on the y axis.

[figure 8]

As expected, the wakes of both models contain large trailing vortices and a central downwash. The square edged model flow-field follows the general form of the Ahmed model wake found by Guilimineau (2008), however, the vortex cores behind the round edged model appear closer to the model centreline and ground plane and this is confirmed in figure 9 that shows the mean vorticity in the wake. In addition to the different vortex locations, the vorticity behind the square edged model configuration is approximately twice as strong and concentrated in a smaller area than in the wake of the round edged model. This increase in vorticity is linked to the stronger local pressure gradients around the sharp edge and the stability of the separation line reduces the motion of the vortex core seen in the downstream wake. The respective vortex strengths are also seen in the differences in the surface pressures on the backlights of the two models. Projecting the vorticity from the round edged model upstream, the location of the vorticity agrees with the small area of low pressure on the trailing edge of the backlight, figure 7, and the flow visualisation on the base, figure 5.

The vorticity behind the square edged model is further from both the ground plane and the centreline leaving space for a separate turbulent, quasi-2D wake behind the model base; this is in agreement with the general flow structure described by Ahmed *et al* (1984) for a sub-critical backlight angle.

[figure 9]

The location of the vorticity behind the round edged model is closer to both the floor and centreline and is where a wake behind the base would be expected rather than a trailing vortex. These results indicate that the trailing vortex and base wake mix producing a different flow structure not described in previously published results where the models typically have defined separation locations around the rear edges.

3.2 Unsteady Results

The structures that exist within the flow fields over both models are, as expected, fundamentally unsteady and consideration of this is vital to fully understand the different flow structures around the two models.

Using the 8192 instantaneous pressure data sets, normal pressure drag and lift and the associated standard deviation of these coefficients has been calculated. As with the steady state results, because of the resolution of the pressure tappings, these values should be treated as indicative rather than as absolute values of the unsteadiness of the forces acting on these faces.

[table 3]

These results show the round edged model has greater unsteadiness in the aerodynamic loads; this is confirmed in figure 10 that shows the pressure fluctuations on the two models. These values are very small and similar to those reported by Bearman and Mullarkey (1994) using a balance and five Davis model configurations.

[figure 10]

On both model configurations there are large surface pressure fluctuations occur towards the backlight header on the model centre line and are larger on the round edged model configuration. This occurs between the two recirculations seen in the flow visualisation at the backlight header and is caused by an unsteady saddle point which agrees with Krajnović and Davidson (2005b) and could be a similar unsteady flow structure as that seen in the notch of a saloon by Gilhome et al (2001) although no dominant frequency could be found in the pressure data. There are also peaks in the pressure fluctuations on the trailing edge of the backlight, as flow separates from the backlight around the curved model edge.
The smallest surface pressure fluctuations occur where the trailing vortices form - on the sides of the model and towards the edges of the backlight.

The RMS fluctuations of the mean in-plane velocity magnitudes, shown as a percentage of freestream velocity, are in figure 11. Note that the large fluctuations in the lower corners of the figure are not a real result, but caused by poor seeding in that small area.

[figure 11]

For both model configurations, the largest velocity fluctuations are associated with the trailing vortex cores and the base wake.
The mixing of the trailing vortices and the wake behind the base of the round edged model is demonstrated by the big, single region of large velocity fluctuations. This contrasts with the square edged model results where the fluctuations from the vortices are distinct from the fluctuations due to the wake behind the model base, albeit with the vortex distorting the wake behind the base and entraining it into the vortex.
The shape of the velocity fluctuations behind the square edged mode agrees with results presented by Lienhart and Becker (2003) in the wake of an Ahmed model with a 25º rear slant.

Mixing of the trailing vortices and wake from the base is further investigated by plotting RMS vorticity fluctuation, figure 12. These results isolate the cause of the unsteady velocities showing which velocity fluctuations are from the trailing vortices.

[figure 12]

In the wake of the round edged model the location of the peak RMS vorticity matches the location of the peak RMS velocity, figure 12, demonstrating that the trailing vortex and wake behind the base are indistinct in the wake of the round edged model. Behind the square edged model the RMS vorticity fluctuations are concentrated in the trailing vortex, shown in the steady state vorticity in figure 9, with significantly lower values present elsewhere. This confirms that the trailing vortex is distinct from the wake behind the base of the model, unlike behind the round edged model.

The differences in the trailing vortices were further investigated by calculating the centre of angular momentum in each of the 1000 instantaneous PIV vector fields using the method of Grosjean *et al* (1997). This calculates the centre of angular momentum in a vector field; if more than one vortex exists only the location of the strongest vortex is recorded. To avoid conflicting results from the left and right trailing vortices, only the left half of the vector field was used. The results of this are shown in figure 13 where the locations of the instantaneous vortex centres are indicated by black dots.

[figure 13]

The locations of the vortex centres for both models agree with the locations of the mean and RMS vorticity in figures 9 and 12 respectively but the round edged model configuration shows a much greater spread indicating a much less stable structure than in the wake of the square edged model. The flow around the rear pillars of the round edged model contains a large component of inboard velocity and minimal vertical velocity. This creates a weak trailing vortex that is close to the surface of the backlight which rolls up into a much larger vortex, mixing with the wake behind the base, when it leaves the backlight. This mixing extends away from the model as the flow from the backlight is carried downstream, hence the wake behind the base close to the model is driven to rotate by the strongly rotating flow downstream, and this explains the weak feature seen in figure 5.
The mixing of the weak trailing vortex and the wake behind the base results in the trailing vortex being located behind the base and the inboard flow component of the flow over the backlight means that the vortex is closer to the model centre line.

The square rear pillars limit the inboard velocity component of the flow into the trailing vortices and create a fixed separation line. This generates strong trailing vortices above the edges of the backlight of the model. Because the trailing vortices are strong and further from the model surface they do not mix with the wake behind the base. This produces stable trailing vortices and a separate wake behind the base which interact though the trailing vortex entraining flow and shearing against the wake behind the base.

3.3 Summary of the Flow Fields

While it is recognised that the flow-field is inherently unsteady for both model geometries, sketches of the inferred, time-averaged flow field are shown in figure 14 for the square edged model and figure 15 for the round edged version. These are useful for comparing with similar published data, particularly to that of Ahmed (1984).

3.3.1 Square Edged Model

[figure 14]

The flow field is generally similar to that described by Ahmed *et al* (1984) with a sub-critical backlight angle. Slight differences occur due to the length of the backlight on the Davis model being longer than on the Ahmed model.
At the backlight header is a complex area of flow recirculation which is the same for both models. This is likely very similar to the flow structures described by Spohn and Gillieron (2002).

The square rear pillars create fixed separation lines along their entire length creating strong vortices above the edges of the backlight. Associated with the strong vortices is a strong central downwash, and the combination of these create high values of drag and lift. The trailing vortices do not mix with the wake behind the base, although they do entrain it. This is the opposite to the situation proposed by Krajnović and Davidson (2005b) and is due to the relative sizes of the model base and backlight on the Ahmed and Davis models. The Davis model creates a stronger vortex and weaker base flow; whereas the larger base and shorter backlight on the Ahmed model create stronger base flows and weaker trailing vortices.
Because the wake behind the base and trailing vortices are distinct the flow structures and hence aerodynamic loads acting on the model are relatively stable.

3.3.2 Round Edged Model

[figure 15]

At the backlight header the complex area of recirculation is the same as found on the square edged model but beyond this the flow structures are quite different from those over the square edged model and that described by Ahmed *et al* (1984) that are often taken as definitive for a fastback. The round rear pillars allow acceleration of the flow from the sides towards the model centre line. For the first 1/3 of the trailing pillar the flow is attached before a separation line develops. This creates trailing vortices that are weak, close to the surface of the model and extend inboard toward the centreline of the model. Upon leaving the backlight, the low and weak trailing vortices mix with the wake behind the base of the model, creating trailing vortices that are behind the base of the model and close to the centre line. This rotation feeds weakly upstream onto the base of the model.
The mixing of the trailing vortices and the wake behind the base is an unsteady process with large variations in the locations of the vortex centres. This unsteady flow structure creates larger unsteady aerodynamic forces acting on the model than on the square edged model.

4. Conclusions

The square edged model produced a flow field very similar to that described by Ahmed *et al* (1984) with separate trailing vortices and wake behind the base, but rounding the rear pillars (with a 10mm radius) created weaker trailing vortices which mix with the wake behind the base of the model changing the overall structure. Consequently, although both models can be described as having a wake dominated by trailing vortices, there are significant differences to both the steady state and unsteady flow fields that have not been described previously. This also shows that the fastback wake structure described by Ahmed is not definitive.

The changes to the wake flow structures demonstrates that the near wake is very dependent upon the curvature of the rear edges of a vehicle, with small changes to the geometry in this region producing disproportionately large changes to the flow field. In addition to fastback shapes, this result is also likely to be applicable to notchback shapes and highlights the lack of published automotive research into the effects of rear edge rounding.

The wake behind the round edged model is more unsteady than that of the square edged model. This is detrimental for vehicle refinement and dynamic stability. In the squared edged case the mean flow field is a more accurate description of the instantaneous flow field than on the more unsteady round edged model meaning that aerodynamic developments can be carried out with greater confidence.

Although adding strakes and flow separation control to the rear edges of production vehicles is often used to reduce drag, these results show that such additions need to be performed with care as they may have unintended

consequences. It is also worth noting that there is no systematic investigation into the effects of changing edge radii of automotive shapes reported in the literature.

The differences in the flow fields shows that the sharp rear edges created stronger and more defined flow structures than those on the round edged model. This leads to the general conclusion that controlling flow separation creates stronger and steadier flow structures than those with a separation line on a curved surface, whilst this is not a new finding, these results confirm this and illustrate its importance in an automotive situation.

5. Acknowledgements

The authors would like to acknowledge the excellent technical assistance provided by Robert Hunter and Stacey Prentice.
We would also like to thank Dan Wood for generating the tubing correction and acknowledge the considerable time and effort taken to find the correction function.

6. References

Ahmed SR, Ramm G, Faltin G (1984) Some Salient Features Of The Time-Averaged Ground Vehicle Wake. SAE Techincal Paper Series, 840300, Detroit MI

Baden Fuller J, Passmore M, Wickern G (2010) An experimental investigation into the transient aerodynamics of a small car using some unsteady test techniques. 8th MIRA International Aerodynamics Conference, Grove, UK, Oct 2010.

Bearman PW (1997) Near wake flows behind two and three - dimensional bluff bodies. Journal of Wind Engineering and Industrail Aerodynamics, Vol 69-71, pages 33-54.

Bearman PW, Mullarkey SP (1994) Aerodynamic Forces on Road Vehicles due to Steady State Side Winds and Gusts, RaeS, Vehicle Aerodynamics Conference, Loughborough

Buresti, G., Fedeli, R., Ferraresi, A., (1997) Influence of afterbody rounding on the pressure drag of an axisymmetrical bluff body. Journal of Wind Engineering and Industrial Aerodynamics, Vol. 69 – 71, Pages 179 - 188

Beaudion, J-F., Aider, J-L., (2008) Drag and lift reduction of a 3D bluff body using flaps. Experiments in Fluids, Vol 44. Pages 491 - 501

Carr GW (1982) Correlation of Aerodynamic Force Measurements in MIRA and Other Automotive Wind Tunnels. SAE Technical Paper Series. 820374. SAE World Congress and Exhibition, Detroit MI.

Davis J (1982) Wind Tunnel Investiagtion of Road Vehicle Wakes. PhD Thesis, Imperial College, London.

Gilhaus, AM, Renn, VE. (1986) Drag and Driving-Stability-Related Aerodynamic Forces and Their Interdependence – Results of Measurements on 3/8 Scale Basic Car Shapes. SAE Techincal Paper Series, 860211, SAE World Congress and Exhibition, Detroit MI.

Gilhome BR, Saunders JW Sheridan J (2001) Time Averaged and Unsteady Near-Wake Analysis of Cars. SAE Technical Paper Series. 2001-01-1040, SAE World Congress and Exhibition, Detroit MI.

Gillerion, P., Chometon, F., (1999) Modelling of Stationary Three-Dimensional Air Flows around an Ahmed Reference Model. Third International Workshop on Vortex. ESAIM Proceedings, Vol 7, pages 173 - 182

Grosjean N et al. (1997) Combining LDA and PIV for turbiulence measurements in unsteady swirling flows. Measurement Science and Technology, Vol. 8, pages 1523-1532.

Guilmineau, E., (2008) Computational study of a flow around a simplified car body. Journal of Wind Engineering and Industrial Aerodynamics. Vol 96, Pages 1207 - 1217

Houghton EL, Carpenter PW (2003) Aerodynamics for Engineering Students, page 264, Butterworth-Heinemann, Oxford. ISBN 0750651113

Howell, JP. (1993) Shape features which influence crosswind stability. Vehicle Ride and Handling Conference, IMechE. Paper C466/036/93, 1993.

Howell JP, Baden Fuller J (2010) A Relationship Between Lift and Lateral Aerodynamic Characteristics for Passenger Cars. SAE Technical Paper Series, 2010-01-1025. SAE World Congress and Exhibition, Detroit MI.

Howell, J., Hickman, D., (1997) The Influence of Ground Simulation on the Aerodynamics of a Simple Car Model. SAE Technical Paper Series, 970134, SAE World Congress and Exhibition, Detroit MI.

Johl G, Passmore M, Render P (2004) Deisgn methodology and performance of an indraft wind tunnel. The Aeronatical Journal, Vol 108, pages 465-473.

Krajnović, S., Davidson, L. (2005) Flow Around a Simplified Car, Part 1 Large Eddy Simulation. Journal of Fluids Engineering. Vol 127, Pages 907 - 918

Krajnović, S., Davidson, L. (2005) Flow Around a Simplified Car, Part 2 Understanding the Flow. Journal of Fluids Engineering. Vol 127, Pages 919 - 928

Lienhart H, Becker S (2003) Flow and Turbulence Structure in the Wake of a Simplified Car Model, SAE Technical Paper Series, 2003-01-0656, SAE World Congress and Exhibition, Detroit MI.

Mansor S (2006) Estimation of Bluff Body Transient Aerodynamic Loads Using an Oscillating Model Rig. PhD Thesis, Loughborough University

Mayer W, Wickern G, (2011) The New Audi A6/A7 Family – Aerodynamic Development of Different Body Types on One Platform, SAE Technical Paper Series, 2011-01-0175, SAE World Congress and Exhibition, Detroit MI.

Morel T, (1978) The Effect of Base Slant on the Flow Pattern and Drag of Three-Dimensional Bodies. In: Sovran G, Morel T Mason Jr WT,. Aerodynamic Drag Mechanisms of Bluff Bodies and Road Vehicles. Plenum Press, pp 191-216, ISBN 0-306-31119-4

Passmore M, Mansor S, (2006) The Measurement of Transient Aerodynamics Using an Oscillating Model Facility. SAE technical Paper Series, 2006-01-0338, SAE World Congress and Exhibition, Detroit MI.

Passmore M, et al. (2010) The Application of Particle Image Velocitmetry in Automotive Aerodynamics. SAE Technical Paper Series, 2010-01-0120, SAE World Congress and Exhibition, Detroit MI.

Sims-Williams DB, Dominy RG (1998) Experimental Investigation into Unsteadiness and Instability in Passenger Car Aerodynamics. SAE Technical Paper Series, 980391, SAE World Congress and Exhibition, Detroit MI.

Sims-Williams DB, Dominy RG, Howell JP (2001) An investigation into Large Scale Unsteady Structures in the Wake of Real and Idealised Hatchback Car Models. SAE Technical Paper Series, 2001-01-1041, SAE World Congress and Exhibition, Detroit MI.

Sims-Williams DB, Duncan B (2003) The Ahmed Model Unsteady Wake: Experiemntal and Computational Analysis. SAE Technical Paper Series, 2003-01-1315, SAE World Congress and Exhibition, Detroit MI.

Sims-Williams DB, Kaye S, Watkins S (2006) Periodic Structures within the Formation Region of Trailing Vortices. SAE Technical Paper Series, 2006-01-1032, SAE World Congress and Exhibition, Detroit MI.

Spohn, A., Gillieron, P. (2002) IUTAM Symposium: Unsteady Separated Flows, Toulouse, France

Figures.

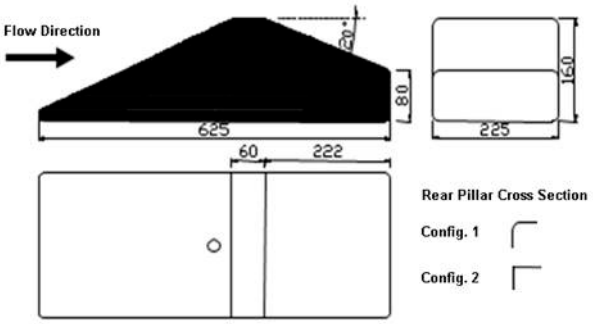

Fig 1 Davis model geometry (dimensions in mm)

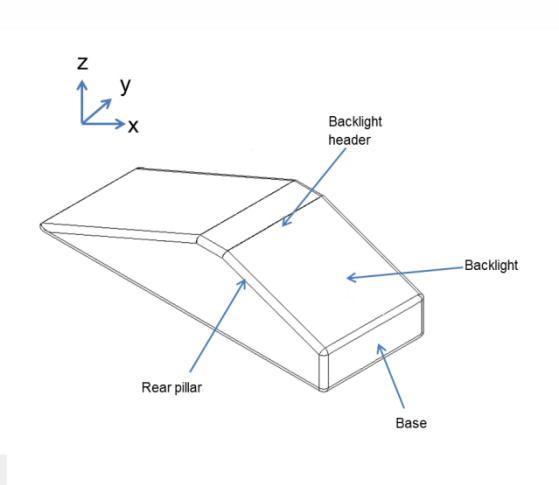

Fig 2 Davis model - annotation of main features

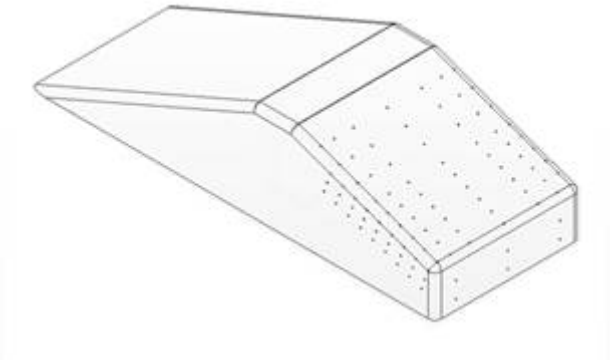

Fig 3 Pressure tapping locations

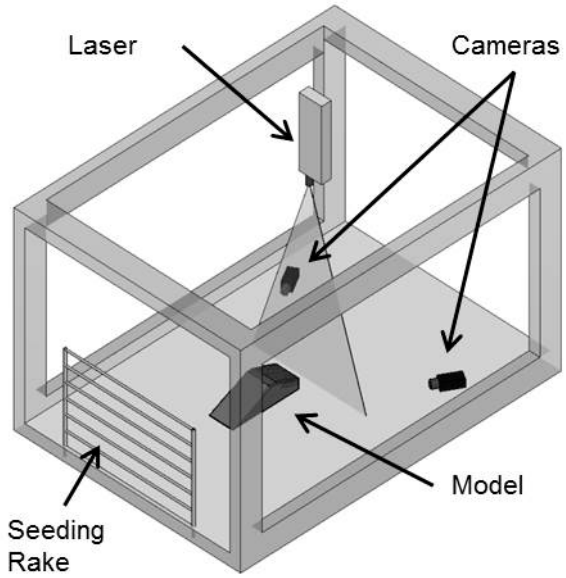

Fig 4 PIV equipment arrangement

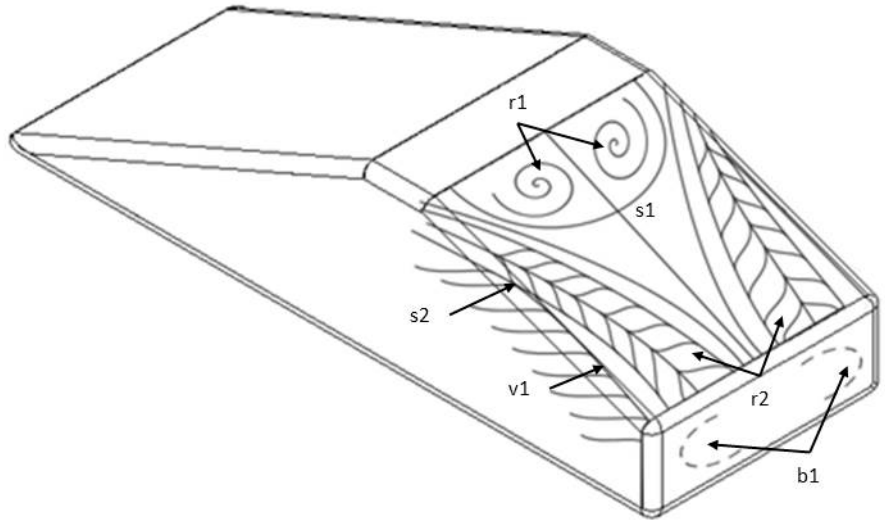

Fig 5 Flow visualisation on the round edged model

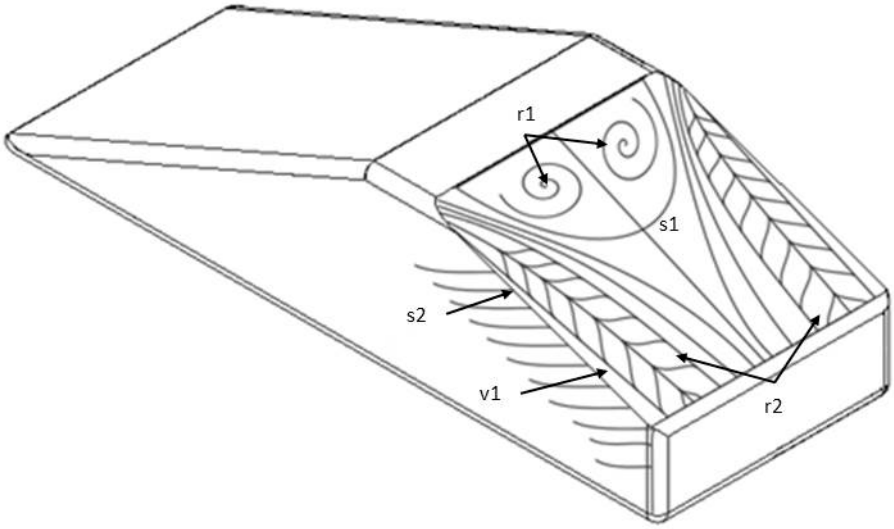

Fig 6 Flow visualisation on square edged model

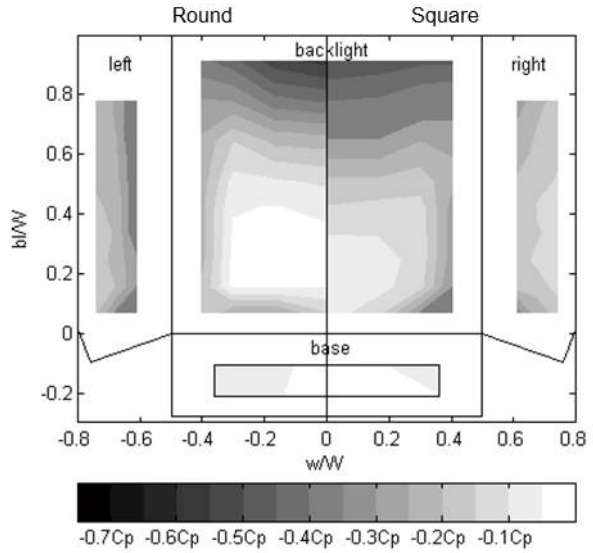

Fig 7 Contours of mean surface pressures, contours in steps of 0.05Cp from -0.75Cp (darker) to 0Cp (lighter)

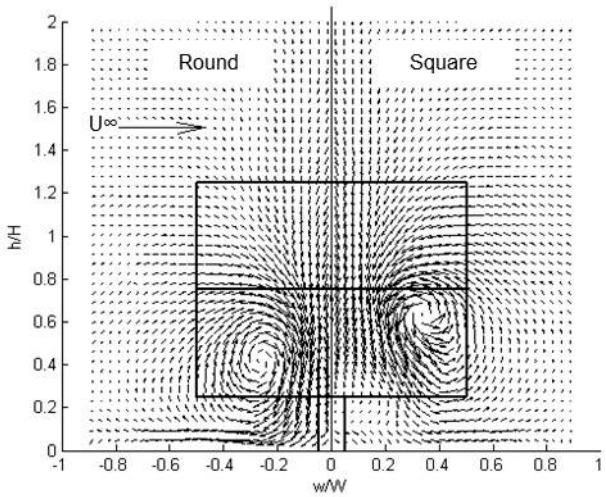

Fig 8 Mean velocity vectors, 0.25L behind the model with freestream velocity shown.

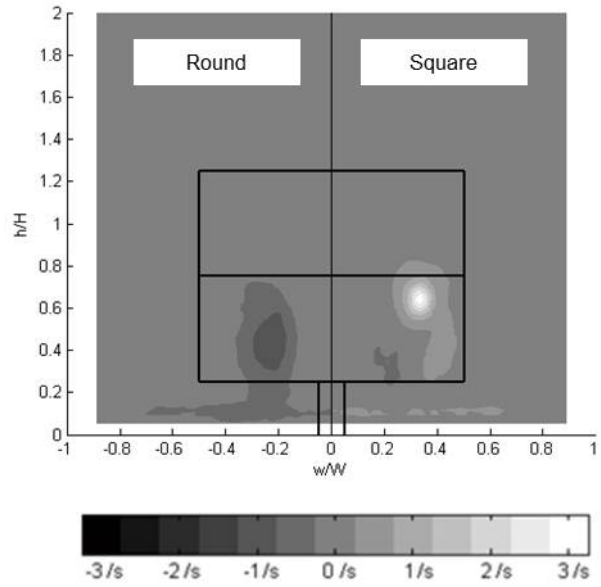

Fig 9 Mean vorticity (1/s), 0.25L behind the model

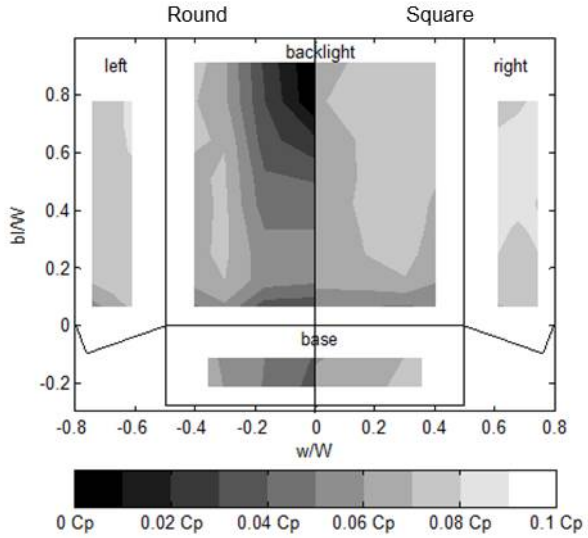

Fig 10 Contours of RMS surface pressures coefficient Cp, from 0 (lighter shades) to 0.1Cp (darker shades)

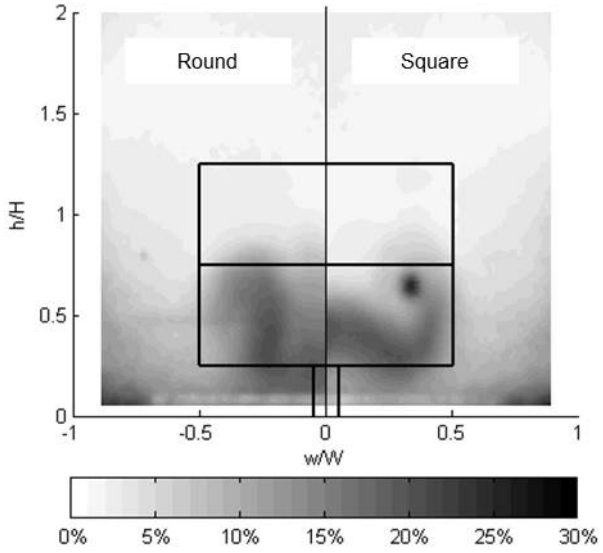

Fig 11 Contours of RMS velocities as a percentage of freestream velocity, from 0% (light shades) to 30% (darker shades)

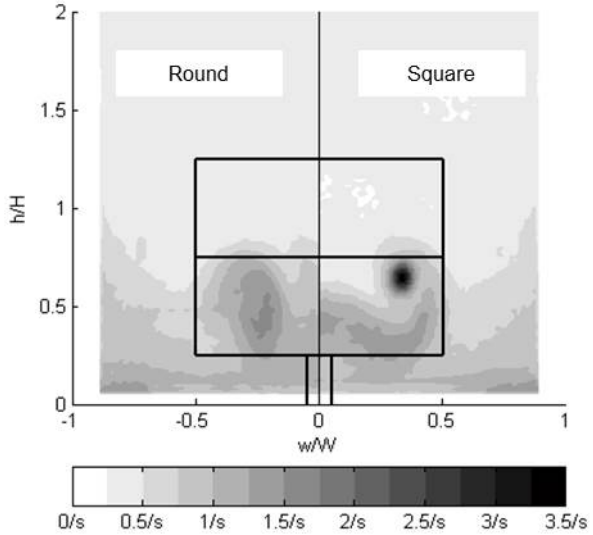

Fig 12 RMS vorticity, from 0/s (light shades) to 3.5/s (darker shades)

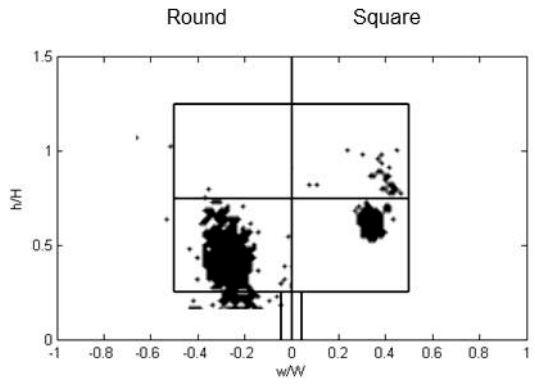

Fig 13 Vortex centre tracking, instantaneous vortex centres indicated by black dots

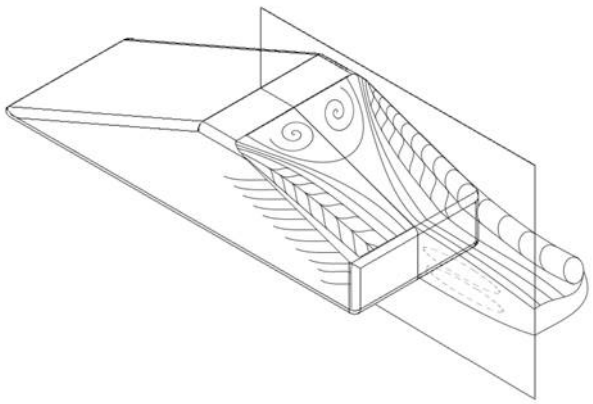

Fig 14 Square edged model flow field

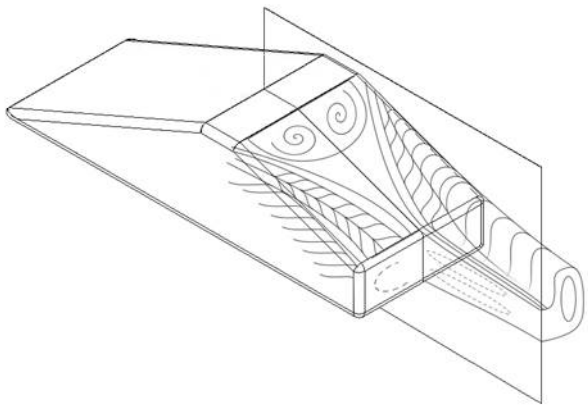

Fig 15 Round edged model flow field

	C_D	C_L	C_{LR}	
Round Edged Model	0.282	0.427	0.388	91%
Square Edged Model	0.317	0.568	0.494	87%

Table 1, Aerodynamic coefficients

	Backlight Lift Coefficient	Backlight Drag Coefficient	Base Drag Coefficient
Round Edged Model	0.254	0.092	0.009
Square Edged Model	0.303	0.110	0.007

Table 2, Force coefficients calculated from surface pressures.

	C_D*	C_L*
Round Edged Model	0.009	0.013
Square Edged Model	0.004	0.007

Table 3, Standard deviation of normal pressure coefficients.